An Asymmetric Model for Quadrupedal Bounding in Place

Romeo Orsolino[1], Michele Focchi[1], Darwin G. Caldwell[1] and Claudio Semini[1]

***Abstract*— In this article we show our approach to determine the main gait parameters of a bounding gait for a quadruped robot. After introducing an asymmetric model that captures the relevant dynamics of quadrupeds we show how this can be employed in an optimization problem that computes a periodic limit cycle. The stability analysis shows that this solution is open loop unstable but can be made marginally stable by means of a state feedback of an augmented system.**

I. Introduction

The problem of legged robot locomotion consists in finding a series of footholds and joint torques which allow to perform a given motion and reach the final target. This study is typically done using simplified dynamic models and then mapping the result to the whole-body dynamics. For humanoids the most widely used simplified model, particularly suitable for highly dynamic motions, is the Spring Loaded Inverted Pendulum (SLIP). In the case of quadruped robots the applicability of this model is limited by their asymmetric structure even when restricted to the 2D sagittal plane. Considering an asymmetric mass distribution is fundamental to describe, for example, the pitch dynamics. A few studies, at the best of our knowledge, of an asymmetric SLIP model can be found in [1], [2], [3] and [4].
The following observations can be made regarding this asymmetry:

- Static measurements on quadruped mammals, mainly dogs and horses, have shown that their Center of Mass (CoM) is always shifted towards the front of the body, resulting in an asymmetric structure. A consequence of this is that front limbs bear around the 60% of the animal's weight in *steady state locomotion* [5], [6].
  The same can happen on quadruped robots which, even if they have a symmetric skeleton, they might be equipped with exteroceptive sensors which are usually positioned in the front to acquire information of the environment in front of the robot.
- Even in the presence of a perfectly symmetric quadruped, the kinematic limits and the manipulability properties of front and hind limbs do not allow them to push or pull their trunk with equal ease in any direction.
- Biological observations have shown that load difference of each limb is tightly connected to their phase difference in the gait cycle [7].

Following the above considerations we decided to employ an asymmetric simplified dynamic model which allows us to design a realistic controller that can be later easily mapped into the full dynamic model of HyQ, IIT's hydraulic quadruped robot [8].

[1]Department of Advanced Robotics, Istituto Italiano di Tecnologia, Via Morego, 30, 16163, Genova, Italy.
email: {romeo.orsolino, michele.focchi, darwin.caldwell, claudio.semini}@iit.it

II. A model for quadrupedal bounding

We designed a 2D dynamic model which could keep this inherent asymmetry into account as depicted in Fig. 1. The impulses J_h and J_f represent the integral of the ground reaction forces (GRFs) F_h and F_f applied to the trunk of the robot during the stance over one cycle by the hind and front legs respectively.

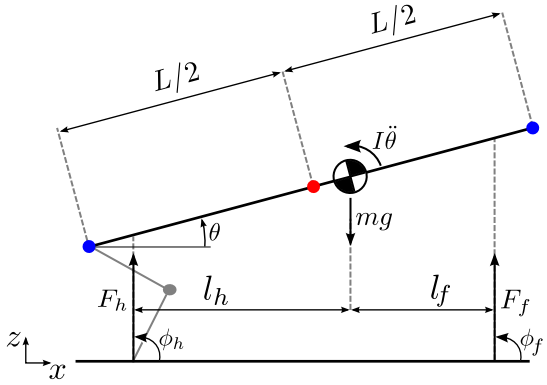

Fig. 1: Snapshot of the simplified planar model of interaction between the trunk of a quadruped robot in the 2D sagittal plane and the ground. The red dot represents the geometric center of the trunk while the blue dots are the two hips.

$$J_h = \int_0^{T_{st}} F_h(t)dt \qquad J_f = \int_0^{T_{st}} F_f(t)dt \tag{1}$$

The lever arms of the GRFs, l_h and l_f, are in general different from the quantity $L/2$ (L is the distance between the hind and front hips) and can be computed as a function of the trunk orientation, the foot contact point and the line of action of the GRFs, defined by the angle ϕ. Here we study the simplified case in which $\phi_h = \phi_f = \pi/2$ in such a way to obtain vertical impulses. The resulting equations of motion are:

$$\begin{aligned} \ddot{x} &= 0 \\ \ddot{z} &= -g + \frac{F_f}{m} + \frac{F_h}{m} \\ \ddot{\theta} &= \frac{F_f}{I} l_f - \frac{F_h}{I} l_h \end{aligned} \tag{2}$$

where I is the inertia of the trunk computed as mr^2, m is the mass and r is the radius of gyration with respect to the CoM [9]. In section III we will use a generalized state vector $\mathbf{q} = [x, \dot{x}, z, \dot{z}, \theta, \dot{\theta}]^T$.

TABLE I: Symbols description

$\mathbf{p}$	3D coordinates of the CoM (x, z, θ)
$\mathbf{q}$	generalized coordinates vector
$\mathbf{q}^*$	fixed point
$\mathbf{q}_{aug}$	augmented state
J_h, J_f	impulse given during stance phase of each leg
F_h, F_f	force profile during stance phase of each leg
ϕ_h, ϕ_f	orientation of the GRFs on the horizontal ground
a_h, a_f	amplitude of the force profile
l_h, l_f	lever arm of the GRFs w.r.t. CoM
d_h, d_k	lever arm of the GRFs w.r.t. hip and knee joints
P	ideal foothold that produces no angular momentum
C_h, C_f	feet position for hind and front legs

A. Pitch dynamics and leg crouching

Highly dynamic gaits which include an aerial phase can be characterized by a non negligible trunk oscillation in the pitch. This oscillation is on one hand a drawback since it implies a certain amount of energy to be spent for a movement which does not directly help the quadruped propel forward. From this point of view if the line of action of the GRF perfectly intersects the CoM this would make the job of moving towards the desired direction more efficiently. On the other hand a certain degree of oscillation is a necessary requirement to make the robot land with the front and hind legs alternately.

Having the line of action of the impulse intersecting the CoM would imply the support foot of the virtual leg to be placed in a point on the ground P far from the standard configuration (Fig. 2a). For quadrupeds, even if the point P is within the leg's kinematic range, this causes the torque to be excessively high at the hip joints, therefore another robot configuration is preferred, that minimizes the effect of the GRFs on the joints (Fig. 2b). Crouching of the legs combined with trunk orientation can help the foot contact point get near the point P (requirement for movements that involve high accelerations, Fig. 2c).

As a final consideration the rocking motion allows to achieve less leg retraction during the swing phase, reducing in this way the risk of stumbling.

B. Foot placement choice

As mentioned above, the lever arms l_h and l_f of the GRFs with respect to the CoM are a function of the feet locations (restricted by the kinematic limits) as well as the orientation of the impulses J_h and J_f. In our strategy we fix the given lever arms l_h and l_f that minimize the torque at the joints by minimizing the lever arms d_h and d_k of the GRFs with respect to the hip and knee joints (see Fig. 2c). Once l_h and l_f are determined in this way, then the feet target location can be easily found with respect to the CoM.

C. Tracking of the Ground Reaction Forces

The main quantities that play a key role in the pitch dynamics are the orientation ϕ, the lever arm l and the amplitude a of the GRFs.

In our model we assume all force profiles to take the form of second order Bezier curves. This force profile is matches well with the GRFs measured from experimental data on humans and quadrupeds and their tracking makes the system robust against ground height, stiffness and damping variations [11]. Specifically for the bounding gait we will have one force

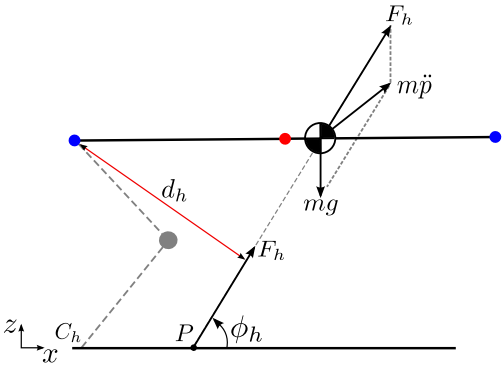

(a) Horizontal trunk and GRF aligned with CoM. The GRFs are applied on the point P and the resulting motion is a pure linear acceleration. It results a large lever arm d_h with respect to the hind hip joint. The point P is far from the standard configuration (grey thick dashed line).

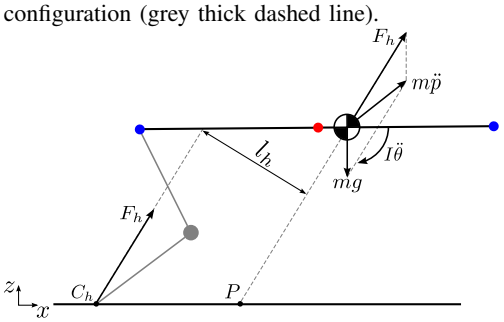

(b) Horizontal trunk and GRF minimizing the lever arm with respect to hind hip and knee joints. The lever arm l_h of F_h with respect to the CoM causes a large negative pitch acceleration $\ddot{\theta}$

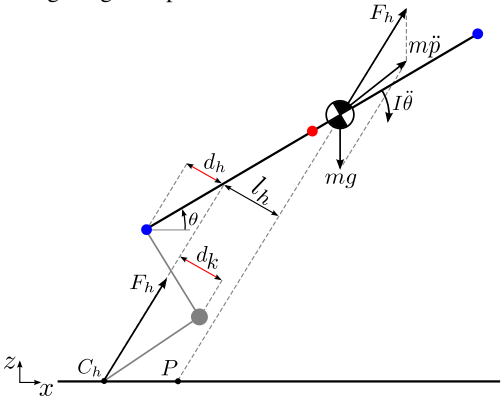

(c) The trunk is inclined of a pitch angle θ and the hind legs are crouched. The point P within the kinematic range of the leg. This allows to concurrently minimize the lever arm l_h of the GRFs with respect to the CoM and the lever arms d_h and d_k with respect to the hip and knee joints.

Fig. 2: Role of pitch orientation and leg crouching in the minimization of the joint torques and in the achievement of the desired rocking motion.

profile for the hind leg and one for the front leg at every cycle, which can be described in this way:

$$F_h : \{l_h, \phi_h, a_h, t_h^{td}\} \quad (3)$$

$$F_f : \{l_f, \phi_f, a_f, t_f^{td}\} \quad (4)$$

where t_f^{td} and t_h^{td} are the scheduled touch-down instants.
We then apply a vertical impulse scaling as introduced by [12] allowing us to find a connection between the impulse amplitude and its time duration - the *stance time* T_{st} - at different horizontal linear speeds.
As mentioned above in this paper we consider only the *vertical dynamics* of the bounding gait, and we thus consider to have $\phi_h = \phi_f = \pi/2$. The resulting vertical desired GRFs are shown in Fig. 3.

III. Selection of the Main Gait Parameters

Thanks to the model defined above describing the interaction between the trunk of the robot and the ground we can completely define an ideal bounding gait by means of a limited set of independent parameters:

- stance time T_{st};
- z coordinate at the apex of the aerial phase z_{apex};
- horizontal speed $\dot{x}$.

We concentrate here on the vertical dynamics meaning that we assume $\dot{x} = 0$. Moreover we assume here a value of z_{apex} of 7 cm which corresponds to about the 10% of the legs length of HyQ, but this value can be changed to increase the foot clearance from the ground in presence, by instance, of obstacles.
The dependent parameters are:

- swing time $T_{sw} = 2\sqrt{\frac{2z_{apex}}{g}}$
- cycle period $T = T_{sw} + T_{st}$
- flight time $T_{fl} = \frac{T - 2T_{st}}{2}$

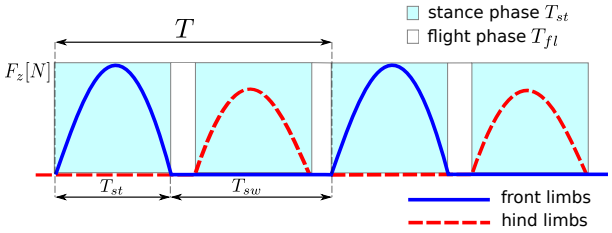

Fig. 3: Desired GRFs of the front (blue) and hind (red) legs in the bounding gait.

A. Discovery of periodic limit cycles

We are now interested in finding the control input and initial states that realize a bounding gait in place for the interaction model described so far. The control input $\mathbf{u}$ represents the desired vertical GRFs for front and hind legs parametrized by the force profiles amplitudes a_f and a_h.
Being the dynamics of the model predefined, these two parameters a_h and a_f represent the optimization variables of this problem together with the initial states $\mathbf{q}_0$. Since we are interested in finding a periodic solution we can arbitrarily choose the initial state of the cycle to be the apex state of the ballistic phase: in this way $z_0 = z_{apex}$ and $x_0 = \dot{x}_0 = \dot{z}_0 = 0$ so that the only free initial states left are θ_0 and $\dot{\theta}_0$.
A periodic limit cycle can be found as a solution of the following optimization problem:

$$\min_{x,u} \quad L(\mathbf{q}, \mathbf{u}) = \int_0^T (\theta^2(t) + \dot{\theta}^2(t) + \mathbf{u}^T(t)\mathbf{u}(t))dt \quad (5)$$

s.t.

- dynamic model: $\dot{\mathbf{q}} = \mathbf{f}(\mathbf{q}, \mathbf{u})$ with: $\mathbf{q} \in \mathbb{R}^{6\times N}$, $\mathbf{u} \in \mathbb{R}^{2\times N}$ and N is the number of integration steps
- periodicity: $\mathbf{q}_0 = \mathbf{q}_N$
- GRFs limits: $0 \leq \mathbf{u} \leq u_{max}$

where $\mathbf{u} = \mathbf{h}(a_h, a_f)$.
The cost function $L(\mathbf{q}, \mathbf{u})$ was chosen in such a way to reduce the rocking motion to the minimum required and to limit the impulse size.

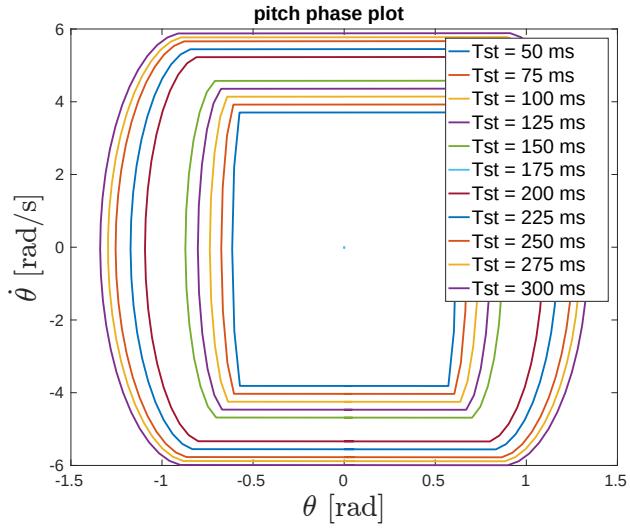

Fig. 4: Different periodic limit cycles found for T_{st} varying between 50 ms and 300 ms (corresponding to duty factors D from 14% to 50%).

In Fig. 4 we see that many periodic limit cycles have been found in the interval of T_{st} between 50 ms and 300 ms for duty factors D between 14% and 50%. We can see that for values of T_{st} higher than 110 ms ($D \simeq 27\%$) we obtain an excessive pitch oscillation of over $\theta \pm 1$ rad; for this reason we restrict our search to the values of T_{st} between 50 ms and 110 ms ($14\% \leq D \leq 27\%$).
Each optimal solution $\mathbf{s}^* = \{\mathbf{q}_0^*, \mathbf{u}^*\}$ will be considered in the next section as a fixed point in a Poincaré map.

B. Stability of the limit cycle

It is now necessary to study the stability of the found periodic limit cycles; this can be done using an approximated Poincaré map. We choose the Poincaré section in coincidence of the apex of the ballistic phase, in this way the solution $\mathbf{s}^*$

represents a fixed point on this map, and we can estimate its stability by perturbing it with a small input error ε_0 and checking the resulting output error ε_T after running a simulation for a whole cycle T [10].
This analysis shows that the x and z dynamics are marginally stable ($\lambda_z = \lambda_z = 1$) while the θ dynamics is unstable ($\lambda_\theta > 1$) for all the analyzed duty factors.
It is now possible to attempt to stabilize the system in two ways:

1) by state feedback;
2) by delaying/anticipating the force impulses.

C. State feedback stabilization of the limit cycle

We employ the first stabilization method which consists in adding a state feedback term to the feedforward term $\mathbf{u}$ composed of the mentioned force profile. The new control input is defined as:

$$\nu = \mathbf{u} - K(\mathbf{q}_0^* - \mathbf{q}_{i,aug}) \tag{6}$$

where $\mathbf{q}_{i,aug} = [\mathbf{q_i}, \mathbf{e}_{i,z}, \mathbf{e}_{i,\theta}]^T$ is the state augmented with two integrators to achieve the tracking of a reference $\mathbf{q}_0^*$. $e_{i,z}$ and $e_{i,\theta}$ are the tracking errors for z and θ respectively:

$$\dot{e}_z = z_0^* - z_i \tag{7}$$

$$\dot{e}_\theta = \theta_0^* - \theta_i \tag{8}$$

$i \in \{0, 1, 2 \dots\}$ is the counter of the latest intersection with the Poincaré section. The gain matrix $K \in \mathbb{R}^{2\times 8}$ can be computed with the discrete LQR technique applied on the linearized Poincaré map A obtained from the fixed point $\mathbf{q}^*$.

$$\dot{\mathbf{q}}_{aug} = \begin{bmatrix} A & 0 & 0 \\ 0 & 1 & 0 \\ 0 & 0 & 1 \end{bmatrix} \mathbf{q}_{aug} + B\mathbf{u} \tag{9}$$

B is determined by measuring the propagation of an error ε_u in the control input to all the states of the system.
Repeating the same Poincaré map analysis on the closed loop system we obtain an improved closed loop behavior where the θ becomes marginally stable like the x and z dynamics. The new closed loop eigenvalues of the linearized map at the fixed point are $\lambda_z = \lambda_\theta = \lambda_x = 1$ for all the considered duty factors.
In Fig. 5 it is possible to see the pitch phase plot in a MATLAB simulation of 10 cycles (above) and the closed loop simulation result compared to the open loop simulation and the optimal solution (below).

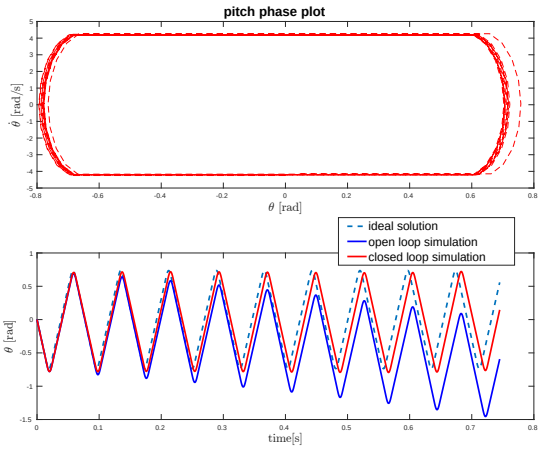

Fig. 5: Phase plot of the pitch dynamics during a 10 cycles simulation (above); evolution of the pitch (red line) compared to the ideal case (dashed line) and to the open loop simulation (blue line) (below).

IV. Conclusion and Future Works

In this paper we have presented a dynamic model and an optimization strategy that allow to compute the main parameters of a periodic bounding gait. The dynamic model is general enough to take the asymmetries of a quadruped animal into account. The optimization finds the optimal periodic solutions depending on the desired T_{st} and z_{apex}. Since the open-loop solutions are unstable, we made the solution marginally stable by state feedback of the augmented state. Future works involve the addition of the horizontal dynamics and the study of the stabilization of the system by means of impulse delay as mentioned in section III-B, as well as the analysis of the robustness of this technique against external disturbances.
This strategy will also be extended to the 3D case to deal with turns and lateral disturbances and to be finally tested on our quadruped robot HyQ.

References

[1] I. Poulakakis and Jesse W. Grizzle*The spring loaded inverted pendulum as the hybrid zero dynamics of an asymmetric hopper*. IEEE Transactions on Automatic Control, 2009.
[2] S.H. Hyon and T. Mita *Development of a biologically inspired hopping robot - Kenken*. ICRA, 2002.
[3] S.H. Hyon and T. Emura *Symmetric Walking Control: Invariance and Global Stability*. ICRA, 2005.
[4] L. Xin, C. Semini and I. Poulakakis *Active Compliance Hybrid Zero Dynamics Control of Bounding on HyQ*. ROBIO, 2015.
[5] L.D. Maes, M. Herbin, R. Hackert, V.L. Bels and A. Abourachid *Steady locomotion in dogs: temporal and associated spatial coordination patterns and the effect of speed.*. The Journal of experimental biology, 2008.
[6] R.M. Walter and D.R. Carrier, *Rapid acceleration in dogs: ground forces and body posture dynamics*. The Journal of experimental biology, 2009.
[7] Y. Fukuoka, Y. Habu and T. Fukui, *A simple rule for quadrupedal gait generation determined by leg loading feedback: a modeling study*. Nature, 2015.
[8] C. Semini, N.G. Tsagarakis, E. Guglielmino, M. Focchi, F. Cannella and D.G. Caldwell, *Design of HyQ - a Hydraulically and Electrically Actuated Quadruped Robot*. IMechE Part I: Journal of Systems and Control Engineering, 2011.
[9] H. Goldstein, *Classical Mechanics*. Addison-Wesley, 1950.
[10] T. S. Parker and L. O. Chua *Practical numerical algorithms for chaotic systems*. Springer, New York, 1989.
[11] D. Koepl and J. Hurst, *Impulse Control for Planar Spring-Mass Running*. Journal of Intelligent and Robotic Systems, 2014.
[12] H.W. Park, Y. Meng, M. Chuah and S. Kim, *Dynamic Quadruped Bounding Control with Duty Cycle Modulation Using Vertical Impulse Scaling*. IROS, 2014.